Influences of light and humidity on carbonyl sulfide-based estimates of photosynthesis

Linda M. J. Kooijmans[a,1,2], Wu Sun[b], Juho Aalto[c,d], Kukka-Maaria Erkkilä[c], Kadmiel Maseyk[e], Ulrike Seibt[b], Timo Vesala[c,f], Ivan Mammarella[c], and Huilin Chen[a,2]

[a]Centre for Isotope Research, University of Groningen, 9747 AG, Groningen, The Netherlands; [b]Department of Atmospheric and Oceanic Sciences, University of California, Los Angeles, CA 90095-1565; [c]Faculty of Science, Institute for Atmospheric and Earth System Research/Physics, University of Helsinki, 00014 Helsinki, Finland; [d]Station for Measuring Forest Ecosystem–Atmosphere Relations II, Hyytiälä Forestry Field Station, University of Helsinki, 35500 Korkeakoski, Finland; [e]School of Environment, Earth and Ecosystem Sciences, The Open University, MK 7 6AA Milton Keynes, United Kingdom; and [f]Faculty of Agriculture and Forestry, Institute for Atmospheric and Earth System Research/Forest Sciences, University of Helsinki, 00014 Helsinki, Finland

Understanding climate controls on gross primary productivity (GPP) is crucial for accurate projections of the future land carbon cycle. Major uncertainties exist due to the challenge in separating GPP and respiration from observations of the carbon dioxide (CO_2) flux. Carbonyl sulfide (COS) has a dominant vegetative sink, and plant COS uptake is used to infer GPP through the leaf relative uptake (LRU) ratio of COS to CO_2 fluxes. However, little is known about variations of LRU under changing environmental conditions and in different phenological stages. We present COS and CO_2 fluxes and LRU of Scots pine branches measured in a boreal forest in Finland during the spring recovery and summer. We find that the diurnal dynamics of COS uptake is mainly controlled by stomatal conductance, but the leaf internal conductance could significantly limit the COS uptake during the daytime and early in the season. LRU varies with light due to the differential light responses of COS and CO_2 uptake, and with vapor pressure deficit (VPD) in the peak growing season, indicating a humidity-induced stomatal control. Our COS-based GPP estimates show that it is essential to incorporate the variability of LRU with environmental variables for accurate estimation of GPP on ecosystem, regional, and global scales.

carbonyl sulfide | photosynthesis | stomatal conductance | carbon cycle

Carbonyl sulfide (COS) follows the same diffusion pathway into the leaf chloroplasts as CO_2 and is consumed by the enzyme carbonic anhydrase (CA) (1, 2). The hydrolysis of COS via CA is irreversible (3), such that no respiration-like COS flux is evident under ambient conditions. Consequently, the atmospheric drawdown of COS above an ecosystem reflects the uptake of COS by plants, provided that other sources and sinks in the ecosystem are negligible or known. The dominant vegetative sink of COS was therefore recognized as a way to separate net ecosystem exchange of CO_2 (NEE) into gross primary productivity (GPP) and respiration (4–7). With a known ratio of COS to CO_2 uptake at the leaf level, GPP can be determined from COS ecosystem fluxes (F_{COS-E}) following (5, 7):

$$GPP_{COS} = -F_{COS-E} \frac{C_{a,CO2}}{C_{a,COS}} \frac{1}{LRU}, \qquad [1]$$

with atmospheric mole fractions $C_{a,COS}$ and $C_{a,CO2}$, and the leaf-scale relative uptake ratio (LRU) = $F_{COS}/F_{CO2} \cdot C_{a,CO2}/C_{a,COS}$, with F_{COS} and F_{CO2} being the flux rates of COS and CO_2 at the leaf level). LRU is also referred to as the ratio of deposition velocities of COS and CO_2 (8). The accuracy of LRU is key in translating COS fluxes into GPP, and several studies have derived LRU for different plant species from chamber enclosure measurements (8–17). Those LRU values ranged from 0.4 to 9.5 with a median of 1.75 and with 50% of the values between 1.48 and 2.46 around the median (see ref. 18 for an overview).

Many of the laboratory studies measured LRU under constant conditions and few have investigated LRU response to environmental variations or under field conditions (13, 17). If effects of light, humidity, and temperature on dissolution, diffusion, and relevant enzyme reactions differ between COS and CO_2, then LRU should be expected to vary (13). It has already been found that LRU changes with light intensity (13, 14, 17, 19, 20). This is due to the light independence of the CA enzyme that controls F_{COS} (14, 21, 22), whereas F_{CO2} depends on the light reactions in the photosystems.

LRU values are typically larger than 1.0, which implies that the deposition velocities of COS are typically higher than those of CO_2. This is attributed to a lower reaction efficiency of ribulose-1,5-bisphosphate carboxylase/oxygenase with CO_2 than that of CA with COS (9, 12), which can be expected because CA is known to be the enzyme with the highest molar activity (2).

Significance

Carbonyl sulfide (COS) measurements enable quantification of terrestrial photosynthesis, which cannot be directly measured at scales greater than the leaf level. The accuracy of COS-based estimates of gross primary production (GPP) depends on how we relate the COS uptake to that of CO_2. This study shows that COS-based GPP estimates will be significantly overestimated if the different environmental responses of COS and CO_2 uptake are not taken into account. These findings are relevant for studies that rely on COS to quantify ecosystem to regional scale GPP, and support the use of a COS-based approach to constrain ecosystem flux partitioning. Moreover, the strong stomatal control on COS uptake shown in this study makes COS a suitable tracer for stomatal diffusion.

Therefore, COS uptake is not expected to be strongly limited by biochemical reactions, unlike CO_2 uptake, which is limited by light reactions in the photosystems. As a result, the stomatal conductance should be a more limiting component for F_{COS} than for F_{CO2}, which makes LRU dependent on stomatal conductance (17). In line with this hypothesis, it has been found that a further decrease of LRU at high radiation levels may occur under conditions of increasing vapor pressure deficit (VPD) and lower stomatal conductance in the afternoon (17). Furthermore, the fact that COS and CO_2 do not share the photochemical reaction in the leaf, but only the diffusive pathway between air and the chloroplast, has recently motivated the use of COS as a tracer for diffusive conductance, of which the stomatal conductance is the dominant component (20, 23).

In this study, we aim to characterize F_{COS} at the branch level under field conditions and investigate if F_{COS} and F_{CO2} respond similarly to environmental changes. We performed continuous COS and CO_2 branch chamber measurements over 5 mo during spring recovery and early summer in 2017 in a boreal forest in Finland, making this a study investigating F_{COS} at the branch level over different phenological stages. This dataset allows us to test the applicability of findings from previous studies—which were confined to laboratory conditions or field measurements over a short period of time—to different phenological stages and environmental conditions. With the different components of F_{COS} (ecosystem, soil, and branch fluxes) being characterized at the site, we are able to derive COS-based GPP estimates and test the effect of the variability of LRU on GPP.

Results and Discussion

Responses of F_{COS} and F_{CO2} to Light and Stomatal Conductance. Both F_{COS} and F_{CO2} show a strong diurnal cycle with a sink during the daytime (Fig. 1A). The increase of COS uptake (more negative F_{COS}) early in the morning coincides with the increase of stomatal conductance ($g_{s,COS}$), whereas the increase of F_{CO2} lags behind due to its light dependence. The peak of F_{COS} is typically 1 h earlier than that of F_{CO2} (Fig. 1A), which was also observed by Geng and Mu (24) in a Chinese deciduous forest. Unlike F_{CO2}, F_{COS} shows continued uptake during nighttime of -1.44 ± 0.95 pmol m^{-2}·s^{-1} (median $\pm$ SD) in May–July (Fig. 1A). The different responses of F_{COS} and F_{CO2} to light is also evident from Fig. 2 A and B; F_{CO2} increases with the photosynthetically active radiation (PAR) up to ~700 μmol m^{-2}·s^{-1}, whereas F_{COS} increases up to a PAR value of ~200 μmol m^{-2}·s^{-1}. The light dependence of F_{CO2} is caused by two distinct processes: (*i*) carbon fixation depends on the light reactions in the photosystems (25) and (*ii*) stomatal aperture, which controls the intercellular CO_2 available for fixation, increases with light as a strategy to optimize carbon gain against water loss (26, 27). In contrast to CO_2, the COS biochemical reactions are light independent (14, 21, 22), but F_{COS} responds to light solely due to the light response of stomatal conductance.

F_{COS} and F_{CO2} peak early in the morning when VPD is still low and $g_{s,COS}$ is high (Fig. 1 A and C), which confirms a shared stomatal control on both fluxes. We find strong correlations of F_{COS} with $g_{s,COS}$ at all light levels and even during night (Fig. 2 E and F). This is strong evidence that F_{COS} could provide a means to constrain stomatal conductance—during both day and night—and therefore links to both the carbon and water cycles (23). However, we also find that, at high light levels, the increase of F_{COS} with $g_{s,COS}$ is smaller than at low light levels (Fig. 2 E and F). This suggests that during the daytime F_{COS} is colimited by nonstomatal resistances, which will be further discussed in the next section.

In the correlation with PAR, we find a decrease of COS uptake (less negative F_{COS}) toward higher light levels (Fig. 2 A and B) that is consistent with a decrease of $g_{s,COS}$ (*SI Appendix*, Fig. S2), while on average F_{CO2} remains constant. This is in line with the hypothesis that the stomatal closure would affect F_{COS} more than it would affect F_{CO2} because the stomatal conductance is a more dominant component for F_{COS} than it is for F_{CO2} (17). This
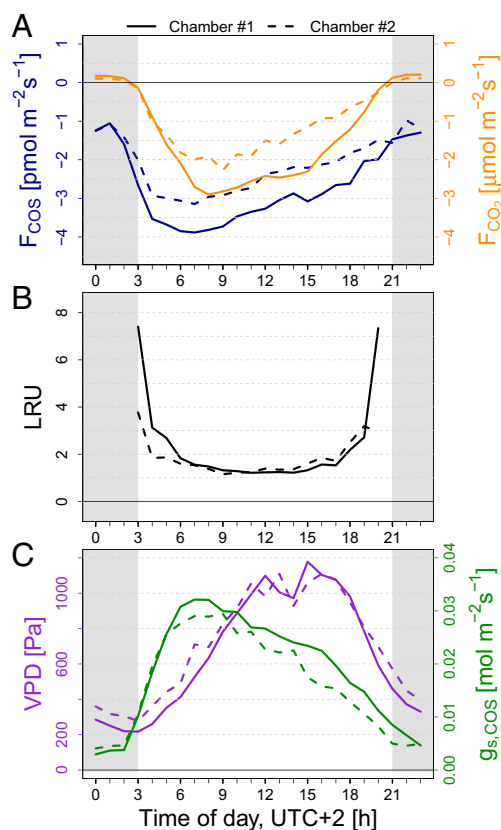
Fig. 1. Average diurnal cycles of F_{COS} and F_{CO2} (*A*), LRU (*B*), and $g_{s,COS}$ and VPD (*C*) between 18 May and 13 July 2017 (the peak season), for chambers 1 (solid) and 2 (dashed). $g_{s,COS}$ is determined in two ways: daytime $g_{s,COS}$ (solar elevation angle > 0°) is determined from the Ball–Berry model, nighttime $g_{s,COS}$ (solar elevation angle < 0°, shaded) is determined from transpiration measurements (*Methods*)—both independent of F_{COS}. We report stomatal conductance as that to COS ($g_{s,COS}$), which relates to stomatal conductance to H_2O ($g_{s,H2O}$) through $g_{s,COS} = g_{s,H2O}/2.00$, where the value 2.00 is the ratio of H_2O and COS diffusivities (12). Time series of F_{COS}, F_{CO2}, LRU, and meteorological parameters can be found in *SI Appendix*, Fig. S1.

may also explain why the peak of F_{COS} occurs earlier than that of F_{CO2} (Fig. 1A); F_{COS} becomes more limited as VPD increases and $g_{s,COS}$ is limited (Fig. 1C), whereas F_{CO2} can continue to increase due to increasing PAR.

LRU varies largely over a day, which reflects the fact that COS uptake is light independent, whereas CO_2 uptake is restricted under low light conditions, e.g., around sunrise and sunset (Fig. 1B). Therefore, LRU decreases exponentially toward high PAR (Fig. 2 C and D), which is similar to the findings in Stimler et al. (14) and Sun et al. (17). The variation of LRU with PAR largely explains the variation of daytime LRU between days (*SI Appendix*, Fig. S1). Moreover, LRU does not become constant toward high light conditions (Fig. 2 C and D, *Insets*), which was also observed by Sun et al. (17) for vegetation in a freshwater marsh. At high light levels we find a correlation between LRU and VPD ($P < 0.01$) and between LRU and $g_{s,COS}$ ($P < 0.05$) in the peak of the growing season (*SI Appendix*, Fig. S3), which is likely due to the different responses of F_{COS} and F_{CO2} to $g_{s,COS}$. These findings support that differential stomatal limitations on F_{COS} and F_{CO2} drive LRU variation.

The light-saturated LRU (for PAR > 700 μmol m^{-2}·s^{-1}) is on average 1.1, which is on the lower end of LRU values reported in previous studies (see ref. 18 for an overview). Note that previous LRU measurements could have been affected by the dependence of LRU to PAR. LRU values have not always been determined at high light levels, which would have led to overestimated LRU. For
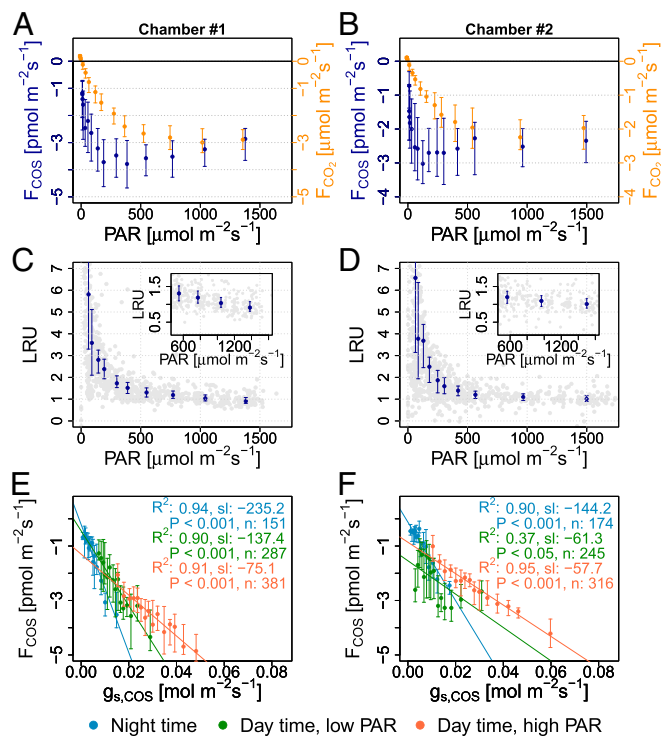
Fig. 2. Responses of F_{COS}, F_{CO_2}, and LRU to light and of F_{COS} to $g_{s,COS}$. Average F_{COS}, F_{CO_2} (*A* and *B*) and LRU (*C* and *D*) versus PAR, and F_{COS} versus $g_{s,COS}$ (*E* and *F*) from 18 May to 13 July for chambers 1 (*Left*) and 2 (*Right*). Data are plotted as the median of 15 equal-sized bins in the *x* range. The error bars represent the 25th and 75th percentiles of data in each bin. For the correlation of F_{COS} with $g_{s,COS}$ (*E* and *F*) the different colors represent different light conditions: nighttime (blue); daytime with low light conditions (PAR < 150 and 100 μmol m^{-2}·s^{-1} for chambers 1 and 2, respectively; green); daytime with high light conditions (PAR > 300 μmol m^{-2}·s^{-1}; orange). A transition phase between low and high PAR values is neglected. The coefficient of determination (R^2), slope (sl), significance level (P), and number of data (n) are given for a linear regression through the median values (*E* and *F*).

example, Kesselmeier and Merk (9) determined LRU at a light level of 300 μmol m^{-2}·s^{-1} and Sandoval-Soto et al. (8) also measured LRU in Scots pine but at a light level of 600 μmol m^{-2}·s^{-1} where F_{CO_2} is not PAR saturated.

Internal Conductance of COS Limits F_{COS} During Daytime. We estimated the internal conductance to COS ($g_{i,COS}$), which is a combination of nonstomatal conductance terms, and find that during daytime $g_{i,COS}$ is smaller than $g_{s,COS}$ (see *SI Appendix*, Fig. S4 and the accompanying explanation). The ratio of $g_{s,COS}$ over $g_{i,COS}$ determines the relative importance of the two conductances on F_{COS} and thereby also on LRU (see equation 8 in ref. 12). The fact that we find a relatively low $g_{i,COS}$ compared with $g_{s,COS}$ during the daytime implies that $g_{i,COS}$ has a relatively large control on F_{COS}. Wehr et al. (23) estimated that the biochemical conductance (the CA activity) was of similar magnitude as $g_{s,COS}$ during the daytime. The fact that we also find a relatively high importance of $g_{i,COS}$ emphasizes the need to take into account $g_{i,COS}$ on the total conductance of COS uptake (17). The day–night difference of $g_{s,COS}$ is larger than that of $g_{i,COS}$, and therefore $g_{s,COS}$ has a relatively larger effect on day–night differences of F_{COS} than $g_{i,COS}$ has. This means that the diurnal change of F_{COS} is largely controlled by $g_{s,COS}$. Furthermore, $g_{i,COS}$ has a relatively larger limiting role on F_{COS} during daytime than during nighttime (*SI Appendix*, Fig. S4). This variable role of $g_{i,COS}$ over a day explains why the relation between F_{COS} and $g_{s,COS}$ is different between different moments of the day, as depicted by different light levels in Fig. 2 *E* and *F*. If F_{COS} is used to determine $g_{s,COS}$,

and the limiting role of $g_{i,COS}$ on F_{COS} is ignored, this would lead to underestimation of daytime $g_{s,COS}$. When the F_{COS}–$g_{s,COS}$ relationship is assumed to be the same for daytime and nighttime (following the blue curve in Fig. 2 *E* and *F*), $g_{s,COS}$ would be equal to 0.012 and 0.020 mol m^{-2}·s^{-1} for chambers 1 and 2, respectively, at F_{COS} of −3 pmol m^{-2}·s^{-1} (the average F_{COS} at high light levels). These values are, respectively, 46% and 48% smaller than what is actually observed (following the orange curve in Fig. 2 *E* and *F*). Therefore, ignoring the role of $g_{i,COS}$ would lead to a substantial underestimation of $g_{s,COS}$.

Seasonal Variation of LRU Influenced by Environmental Variables. Fig. 3 shows the light-saturated LRU per month binned by VPD. The monthly median LRU decreases by 0.2 from April to July. No significant correlation between LRU and VPD can be detected before June, whereas a significant decrease of LRU with VPD is observed in June and July (indicated by the significance levels in Fig. 3). The fact that the LRU–VPD correlation follows the progression of the growing season is associated with the increase of daytime VPD. Early in the season F_{COS} and F_{CO_2} are not solely limited by stomatal conductance but rather by low temperatures, as is shown in *SI Appendix*, Fig. S5. The low temperatures suppress enzyme activities or mesophyll diffusion and therefore $g_{i,COS}$ has a relatively larger limiting effect on F_{COS} than $g_{s,COS}$ early in the season. In the course of the season the limitation of VPD on stomatal conductance becomes stronger, which manifests in the LRU–VPD relationship. This emphasizes that the LRU–$g_{s,COS}$ correlation (*SI Appendix*, Fig. S3) only applies when both F_{COS} and F_{CO_2} are controlled by stomatal conductance; i.e., at high temperatures and high light conditions.

Light and Humidity-Dependent LRU Required for Accurate COS-Based GPP Estimates. In Fig. 4 we compare COS-based GPP estimates (GPP$_{COS}$) from COS ecosystem fluxes (determined from eddy-covariance measurements and subtracted estimates of the soil flux) with GPP from a traditional flux-partitioning method based on extrapolating nighttime respiration to the daytime (28) (GPP$_{NEE}$). GPP$_{COS}$ is determined using different parameterizations of LRU: (*i*) a fit of the measured LRU (averaged over chambers 1 and 2) against PAR, which captures the decrease of LRU toward simultaneously increasing VPD and PAR (GPP$_{COS-fit}$; see *SI Appendix*, Fig. S6 for the LRU–PAR relationship) and (*ii*) LRU fixed at 1.1 (the average LRU that we find at high light levels) and 1.6 [similar to what has been frequently used in other literature (7, 15, 29)], where the latter is shown in Fig. 4 as GPP$_{COS-const}$. The shading of the GPP estimates represents the uncertainty based on Monte Carlo sampling of all parameters contributing to the GPP calculations (*Methods*). The GPP$_{COS}$ uncertainty is larger than that of GPP$_{NEE}$, partly because the relative uncertainty of COS mole fraction measurements (∼1.7% of a typical ambient level of 450 ppt) is greater than that of CO_2 mole fraction measurements (∼0.06% of a typical value of 400 ppm) (30). Still, Fig. 4 shows that the accuracy of GPP$_{COS}$ is sufficient to detect differences between GPP$_{COS}$ and GPP$_{NEE}$. We also calculated GPP$_{COS}$ with the measured hourly LRU to determine to what extent uncertainty in the LRU–PAR function adds uncertainty to GPP$_{COS-fit}$. The uncertainties did not decrease with measured LRU values compared with the LRU–PAR function, implying that the empirical function captures the variability of LRU over the measurement period well.

With the constant LRU, the earlier peak of F_{COS} leads to an earlier peak in GPP$_{COS-const}$ compared with GPP$_{NEE}$. The peak of ecosystem F_{COS}, and thus that of GPP$_{COS-const}$, is 2 h later than the peak of F_{COS} measured at the branch level at the top of the canopy. The reason for the delay between the F_{COS} peak from branches and ecosystem is that the diurnal pattern of the bulk canopy conductance is more symmetric, because light rather than g_s is limiting CO_2 assimilation in the lower canopy, in contrast to the top of the canopy (31). When GPP$_{COS}$ is calculated with the average LRU that we find at high light levels (1.1), we find GPP$_{COS}$ (13.4 ± 1.3 g C m^{-2}·d^{-1}; daytime data only) to

Kooijmans et al.

Fig. 3. Seasonal variation of light-saturated LRU. (*Top*) LRU per month plotted as the median of three equal-sized bins of VPD (kPa) for chamber 1 (*Left*) and chamber 2 (*Right*). Only data above the light saturation point of F_{CO2}, i.e., 700 µmol m^{-2}·s^{-1}, are included to minimize the effect of PAR on LRU. The month of February is not included because in that month PAR does not reach values above 700 µmol m^{-2}·s^{-1}. The error bars represent the 25th and 75th percentiles of data in each bin. The median LRU of all VPD classes is plotted per month in gray. Significance levels (P) of linear regressions of LRU against VPD are given per month. (*Bottom*) The number of data in each bin.

be overestimated by 72% compared with GPP$_{COS\text{-}fit}$. A fixed LRU value of 1.1 is not even sufficient for peak daytime values of GPP$_{COS}$, because cloudy days would have lower PAR, leading to higher LRU and lower GPP$_{COS}$. When GPP$_{COS\text{-}const}$ is based on the LRU value that is frequently used in other studies (1.6), GPP$_{COS}$ is underestimated at high light levels, but overestimated in the early morning and late afternoon (Fig. 4) with the daytime sum being 7% overestimated compared with GPP$_{COS\text{-}fit}$ (daytime data only). These comparisons demonstrate that a constant LRU does not capture the variability of GPP. To the contrary, the diurnal cycles of GPP$_{NEE}$ and GPP$_{COS\text{-}fit}$ track closely in the early morning and late afternoon. The sum of daily GPP estimates differ by 13% (6.8 ± 0.3 and 7.8 ± 0.9 g C m^{-2}·d^{-1} for GPP$_{NEE}$ and GPP$_{COS\text{-}fit}$, respectively). If LRU is held constant at a too-high value toward high PAR—when the different response of F_{COS} and F_{CO2} to stomatal closure is ignored—this would lead to an underestimation of GPP during daytime.

Ideally, COS would be used to validate other flux-partitioning methods and to assess assumed relations, such as the relation between respiration and temperature that is used to determine GPP$_{NEE}$ (28). Recent studies in a temperate deciduous forest and an Arctic tundra have found that the standard flux-partitioning technique typically overestimates daytime ecosystem respiration and thereby overestimates GPP (32, 33). Here we find that GPP$_{COS\text{-}fit}$ is 13% higher than GPP$_{NEE}$. The separation between GPP$_{COS\text{-}fit}$ and GPP$_{NEE}$ around noon that is larger than the uncertainty (Fig. 4) shows that GPP$_{COS\text{-}fit}$ can be used to detect biases in other methods. However, the LRU that we used to calculate GPP$_{COS\text{-}fit}$ is based on PAR levels at the top of the canopy and does not account for lower PAR levels within the canopy. Accounting for a lower PAR within the canopy is expected to result in a higher canopy-integrated LRU and lower GPP$_{COS\text{-}fit}$ than those currently shown in Fig. 4. The extent to which GPP$_{COS}$ would decrease, and how it then compares with GPP$_{NEE}$, would have to be investigated by taking into account the canopy profiles of leaf area density and light attenuation and the empirical LRU–PAR relation that is found in this study. It also has to be tested from field measurements how LRU behaves under different light regimes within the canopy, where light-use efficiency can be higher for diffuse radiation than for direct radiation (34). The current GPP$_{COS}$ estimate does not allow for drawing conclusions about the bias of GPP in other methods, but the current state of knowledge is not far from application of COS as a tool to cross-validate other flux-partitioning methods.

The Implications in Large-Scale GPP Estimates. The application of COS as a GPP tracer in terrestrial biosphere models can make use of LRU to scale the COS vegetation fluxes to those of CO_2. The relationships of LRU with PAR and VPD that are presented in this study are needed to make sure that the diurnal and seasonal variability of LRU is accounted for in terrestrial biosphere models (36–38). With accurate representation of LRU, the use of COS could potentially help improve the representation of diurnal variations of GPP in such models (29, 38). Furthermore, a time-integrated LRU is a useful measure to make the link between plant COS uptake and gross CO_2 uptake when large-scale biosphere models do not resolve diurnal cycles. For the months May–July we find that the time-integrated ratio of COS and CO_2 deposition velocities (based on branch measurements) is 1.6 (daytime only); including the months February–April the value is equal to 2.0 due to lower light conditions early in the season (*SI Appendix*, Fig. S7). Taking into account the nighttime data, the time-integrated F_{COS} to F_{CO2} ratio is 1.9 and 5.3 for May–July and February–July, respectively. These values apply to the branch level, in this case particularly to branches at the top of the canopy. For an accurate conversion of F_{COS} to GPP on the ecosystem and regional scales one needs to account for vertically varying PAR levels within the canopy. Furthermore, for upscaling to regional and global scales, the LRU–PAR relationship would have to be determined for other plant species in different ecosystems, given that large variability in LRU has previously been found between plant species (8, 12, 14–16, 39). For example, nighttime COS uptake by vegetation was shown to be small in a Mediterranean climate (39), leading to lower variation of LRU with PAR than what we found in this study for a boreal forest. These differences in LRU response in different climatic regions show that results from LRU dependencies in a single biome cannot be generalized across different climatic regions.

Moreover, the strong relationship between F_{COS} and g_s that was shown in this study can be used in process-based modeling studies to constrain the CO_2 diffusion pathway. Large improvements can be made particularly on the extent of nighttime stomatal opening, which is otherwise poorly quantified.

Conclusion

The different responses of F_{COS} and F_{CO2} to environmental variables, especially light, should not be ignored when COS flux measurements (either at leaf, ecosystem, regional, or global scales) are used to interpret changes in photosynthetic CO_2 uptake. Our findings show that the strong variability of LRU

Fig. 4. GPP estimates based on COS and standard methods. Diurnal cycles of GPP between 18 May and 13 July 2017 based on NEE partitioning (GPP$_{NEE}$; red) and observed COS ecosystem fluxes [using EC measurements with soil flux estimates subtracted (45)] following Eq. **1** (GPP$_{COS}$). For GPP$_{COS}$, LRU is determined with two different representations: from a PAR-dependent fit (*SI Appendix*, Fig. S6) of LRU based on the continuous branch measurements, where the average of chambers 1 and 2 is taken (GPP$_{COS-fit}$; blue); LRU fixed at 1.6 (GPP$_{COS-const}$; green), which is similar to what has been frequently used in other literature (7, 15, 29). The averages (thick lines) and uncertainties (shaded areas) are based on 1,000 subsamples of Monte Carlo simulations that include uncertainties of all contributing components in the GPP calculation in each bin (*Methods*). We calculated the summed GPP from the average diurnal cycle for each representation (for daytime data only), which is shown in the top right corner.

with environmental variables and phenological stages must be incorporated to obtain accurate estimates of GPP from COS measurements. The LRU–PAR relationship found in this study can help to scale up LRU to ecosystem, regional, and global scales. Furthermore, the close relationship between F$_{COS}$ and g$_s$ that we observed can provide additional constraints to both the carbon and water cycles. With recent efforts to characterize sources and sinks of COS in ecosystems, accurate COS-based GPP estimates are now within reach and will allow testing and validation of other flux-partitioning methods.

Methods

Branch Measurements. Measurements were performed at the Station for Measuring Ecosystem–Atmosphere Relations II (SMEAR II) in Hyytiälä, Finland (61°51′ N, 24°17′ E, 181 m above sea level), which is dominated by Scots pine (*Pinus sylvestris L.*) (40). Four automated gas-exchange chambers were installed at the top of the canopy in two Scots pine trees between February 16 and July 17, 2017; details of those chamber meausurements are provided in *SI Appendix*. PAR was measured by quantum sensors (Li-Cor LI-190) inside and outside the chambers. Temperature sensors (thermocouples and PT100) were placed inside the chambers. During measurements, the chambers were closed for 4 min and each chamber was measured once every hour. Air was pumped through a 4-mm (inner) diameter Synflex (Decabon) tube of 65-m length from the branch chambers to a quantum cascade laser spectrometer (QCLS) (Aerodyne Research Inc.) with a flow of 1–1.5 L min^{-1} which was constantly recorded with Honeywell flowmeters (AWM5101VN). No active supply flow was provided, but ambient air could enter the chamber through small holes in the chamber housing (41). The sample tubing outside the instrumentation cabin was heated to prevent condensation on the tubing walls. The QCLS measured COS, CO$_2$, CO, and H$_2$O mole fractions (1 Hz) from the branch chambers along with half-hourly cylinder measurements for calibration. We corrected for the spectral water vapor interference of COS (30). The overall uncertainty including scale transfer, water vapor corrections, and measurement precision was determined to be 7.5 parts per trillion for COS and 0.23 parts per million for CO$_2$ (30). More information about the instrumentation and the calibration method can be found in Kooijmans

et al. (30) and the deployment of the instrument at the SMEAR II station in Kooijmans et al. (42).

Fluxes were calculated from the change of molar concentrations within the chamber during chamber closure through the following mass balance equation:

$$V \frac{dC}{dt} = FA + q(C_a - C),$$ [2]

where C is the molar concentration of each species inside the chamber (mol m^{-3}), C$_a$ the ambient molar concentration (mol m^{-3}), V the chamber volume (m^3), F the uptake or emission rate (mol m^{-2}·s^{-1}), A the leaf area (m^2), and q the flow rate (m^3 s^{-1}). The measured mole fractions of the gas species (mol mol^{-1}) are converted to molar concentrations using the ideal gas law with average temperature during chamber closure and pressure measurements at the site. The fluxes were calculated from least-square fit of the time series of molar concentrations inside the chamber and by solving Eq. **2**. C$_a$ was determined from open chamber measurements during a few minutes before chamber closure.

We measured fluxes in empty chambers (called "blank" measurements) to test and correct for gas exchange by the chamber and possibly by tubing materials. We measured blanks for all chambers in July and during a few days in March, May, and June. The fluxes were corrected for the blank emissions as is further described in *SI Appendix*.

In *SI Appendix* we also discuss the effect of leaf mitochondrial respiration on F$_{CO2}$ and LRU. Since we do not have the means to quantify diurnal changes of leaf mitochondrial respiration we approximate leaf-level LRU with the observed F$_{CO2}$.

Stomatal Conductance. With transpiration measurements (F$_{H2O}$) available, we would ideally calculate stomatal conductance to water vapor (g$_{s,H2O}$) from F$_{H2O}$ normalized by VPD, where F$_{H2O}$ is simultaneously determined along with F$_{COS}$ and F$_{CO2}$ from the branch chamber measurements. However, in chamber measurements, transpiration is underestimated at high relative humidity (RH) levels because the transpired water vapor can get adsorbed on the chamber walls. Measurements of F$_{H2O}$ therefore may not provide reliable g$_{s,H2O}$ estimates at high humidity levels. Therefore, we determined g$_{s,H2O}$ from the Ball–Berry model where the empirical slope (m) and intercept (g$_0$) parameters are determined from g$_{s-H2O}$, which is determined with F$_{H2O}$ and VPD under low-humidity conditions. We use a threshold for RH (70%) to avoid the effect of condensation on the chamber walls. The Ball–Berry model describes g$_{s,H2O}$ as function of F$_{CO2}$, RH and the atmospheric CO$_2$ mole fraction (43):

$$g_{s,H2O} = m \cdot F_{CO2} \cdot \frac{RH}{C_{a,CO2}} + g_0.$$ [3]

The model parameters m and g$_0$ are determined through linear regression with an R^2 of 0.98 and 0.99 for chambers 1 and 2, respectively. With the regression being linear, we do not expect that using the Ball–Berry model rather than the measured g$_{s,H2O}$ leads to a bias in the results. As the Ball–Berry model does not allow for g$_{s,H2O}$ estimates in the dark when there is no photosynthesis, we determined the nighttime g$_{s,H2O}$ based on F$_{H2O}$ normalized by VPD (for RH < 70%). The leaf temperature used for VPD was calculated from a leaf energy balance model that incorporated heating by incoming shortwave radiation and cooling by transpiration and sensible heat transfer (44). The RH used for VPD calculations was determined from water vapor mole fractions in the open chamber a few minutes before chamber closure.

GPP Estimates. We determined GPP from NEE and extrapolated nighttime respiration following the traditional flux-partitioning method in Reichstein et al. (28). In addition to these NEE-based GPP estimates, we calculated GPP through Eq. **1** using different representations of LRU: with a PAR-dependent fit to the measured LRU (*SI Appendix*, Fig. S6) and with LRU fixed at 1.1 and 1.6. Vegetative COS fluxes were determined from eddy-covariance (EC) measurements in 2017 and soil COS fluxes that were characterized at the site in 2015 (45). The EC measurements of COS fluxes were made with a second QCLS of the same make at 10-Hz frequency together with a sonic anemometer (Solent Research HS1199; Gill Ltd.) at 23-m height. EC fluxes of COS were calculated from COS mixing ratios (corrected for water vapor in air) using the EddyUH software package developed at the University of Helsinki (46). Storage fluxes were estimated from mole fractions at 18 m assuming a constant height profile. More details about the flux and storage calculation procedure can be found in Kooijmans et al. (42). Data with low friction velocity (<0.3 m·s^{-1}) were filtered out. Soil COS fluxes were measured in 2015 at the Hyytiälä site and showed no seasonal or diurnal cycle (45). An average

soil flux of -2.7 pmol m$^{-2}\cdot$s^{-1} was subtracted from the ecosystem fluxes such that the remaining flux represents the vegetative COS exchange. The averages and uncertainties shown in Fig. 4 are based on 1,000 subsamples of Monte Carlo simulations that include uncertainties of all contributing components in the GPP calculation. That is, the SE of F_{COS-EC} and NEE; the COS soil flux uncertainty of 1.1 pmol m$^{-2}\cdot$s^{-1} (45); the SE of the fitting parameters of the LRU-PAR relation (using the median PAR in the calculation), or no uncertainty in LRU in the case of a constant LRU; the uncertainties of COS and CO_2 mole fractions of 6.0 ppt and 0.13 ppm respectively (30), and the range of respiration calculations from figure 11 in ref. 47.

Meteorological Data. In addition to the temperature and PAR sensors installed at the branch chambers we use the data that are made available through the SmartSMEAR database that contains continuous data records from all SMEAR sites (available at https://avaa.tdata.fi/).

Statistical Tests. The significance of correlations is tested with two-sided t tests of which the significance levels (P) are reported. To reduce the effect of outliers we test the linear correlation of data based on bin-averaged medians, where the bins are of equal size. The number of samples of the original data are reported for each t test. The number of bins are mentioned in figure legends.

Code and Data Availability. Data and code related to this paper are available in refs. 48–50.

EARTH, ATMOSPHERIC, AND PLANETARY SCIENCES

1. Protoschill-Krebs G, Wilhelm C, Kesselmeier J (1992) Enzymatic pathways for the consumption of carbonyl sulphide (COS) by higher plants. *Bot Acta* 105:206–212.
2. Protoschill-Krebs G, Wilhelm C, Kesselmeier J (1996) Consumption of carbonyl sulphide (COS) by higher plant carbonic anhydrase (CA). *Atmos Environ* 30:3151–3156.
3. Notni J, Schenk S, Protoschill-Krebs G, Kesselmeier J, Anders E (2007) The missing link in COS metabolism: A model study on the reactivation of carbonic anhydrase from its hydrosulfide analogue. *Chembiochem* 8:530–536.
4. Montzka SA, et al. (2007) On the global distribution, seasonality, and budget of atmospheric carbonyl sulfide (COS) and some similarities to CO2. *J Geophys Res Atmos* 112:D09302.
5. Campbell JE, et al. (2008) Photosynthetic control of atmospheric carbonyl sulfide during the growing season. *Science* 322:1085–1088.
6. Berry J, et al. (2013) A coupled model of the global cycles of carbonyl sulfide and CO2: A possible new window on the carbon cycle. *J Geophys Res Biogeosci* 118:842–852.
7. Asaf D, et al. (2013) Ecosystem photosynthesis inferred from measurements of carbonyl sulphide flux. *Nat Geosci* 6:186–190.
8. Sandoval-Soto L, et al. (2005) Global uptake of carbonyl sulfide (COS) by terrestrial vegetation: Estimates corrected by deposition velocities normalized to the uptake of carbon dioxide (CO2). *Biogeosciences* 2:125–132.
9. Kesselmeier J, Merk L (1993) Exchange of carbonyl sulfide (COS) between agricultural plants and the atmosphere: Studies on the deposition of COS to peas, corn and rapeseed. *Biogeochemistry* 23:47–59.
10. Kesselmeier J, et al. (1993) Reduced sulfur compound exchange between the atmosphere and tropical tree species in Southern Cameroon. *Biogeochemistry* 23:23–45.
11. Kuhn U, et al. (1999) Carbonyl sulfide exchange on an ecosystem scale: Soil represents a dominant sink for atmospheric COS. *Atmos Environ* 33:995–1008.
12. Seibt U, Kesselmeier J, Sandoval-Soto L, Kuhn U, Berry JA (2010) A kinetic analysis of leaf uptake of COS and its relation to transpiration, photosynthesis and carbon isotope fractionation. *Biogeosciences* 7:333–341.
13. Stimler K, Montzka SA, Berry JA, Rudich Y, Yakir D (2010) Relationships between carbonyl sulfide (COS) and CO2 during leaf gas exchange. *New Phytol* 186:869–878.
14. Stimler K, Berry JA, Montzka SA, Yakir D (2011) Association between carbonyl sulfide uptake and (18)Δ during gas exchange in C(3) and C(4) leaves. *Plant Physiol* 157:509–517.
15. Stimler K, Berry JA, Yakir D (2012) Effects of carbonyl sulfide and carbonic anhydrase on stomatal conductance. *Plant Physiol* 158:524–530.
16. Berkelhammer M, et al. (2014) Constraining surface carbon fluxes using in situ measurements of carbonyl sulfide and carbon dioxide. *Global Biogeochem Cycles* 28:161–179.
17. Sun W, Maseyk K, Lett C, Seibt U (2018) Stomatal control of leaf fluxes of carbonyl sulfide and CO2 in a Typha freshwater marsh. *Biogeosciences* 15:3277–3291.
18. Whelan ME, et al. (2018) Reviews and syntheses: Carbonyl sulfide as a multi-scale tracer for carbon and water cycles. *Biogeosciences* 15:3625–3657.
19. Maseyk K, et al. (2014) Sources and sinks of carbonyl sulfide in an agricultural field in the Southern Great Plains. *Proc Natl Acad Sci USA* 111:9064–9069.
20. Commane R, et al. (2015) Seasonal fluxes of carbonyl sulfide in a midlatitude forest. *Proc Natl Acad Sci USA* 112:14162–14167.
21. Gries C, Nash TH, Kesselmeier J (1994) Exchange of reduced sulfur gases between lichens and the atmosphere. *Biogeochemistry* 26:25–39.
22. Protoschill-Krebs G, Wilhelm C, Kesselmeier J (1995) Consumption of carbonyl sulphide by chlamydomonas reinhardtii with different activities of carbonic anhydrase (CA) induced by different CO2 growing regimes. *Bot Acta* 108:445–448.
23. Wehr R, et al. (2017) Dynamics of canopy stomatal conductance, transpiration, and evaporation in a temperate deciduous forest, validated by carbonyl sulfide uptake. *Biogeosciences* 14:389–401.
24. Geng C, Mu Y (2006) Carbonyl sulfide and dimethyl sulfide exchange between trees and the atmosphere. *Atmos Environ* 40:1373–1383.
25. Farquhar GD, von Caemmerer S, Berry JA (1980) A biochemical model of photosynthetic CO2 assimilation in leaves of C 3 species. *Planta* 149:78–90.
26. Cowan IR, Farquhar GD (1977) Stomatal function in relation to leaf metabolism and environment. *Symp Soc Exp Biol* 31:471–505.
27. Farquhar GD (1982) Stomatal conductance and photosynthesis. *Annu Rev Plant Physiol* 33:317–345.

28. Reichstein M, et al. (2005) On the separation of net ecosystem exchange into assimilation and ecosystem respiration: Review and improved algorithm. *Glob Change Biol* 11:1424–1439.
29. Hilton T, et al. (2017) Peak growing season gross uptake of carbon in North America is largest in the Midwest USA. *Nat Clim Chang* 7:450–454.
30. Kooijmans LMJ, et al. (2016) Continuous and high-precision atmospheric concentration measurements of COS, CO2, CO and H2O using a quantum cascade laser spectrometer (QCLS). *Atmos Meas Tech* 9:5293–5314.
31. Launiainen S, Katul GG, Kolari P, Vesala T, Hari P (2011) Empirical and optimal stomatal controls on leaf and ecosystem level CO2 and H2O exchange rates. *Agric For Meteorol* 151:1672–1689.
32. Wehr R, et al. (2016) Seasonality of temperate forest photosynthesis and daytime respiration. *Nature* 534:680–683.
33. Wilkman E, et al. (2018) Temperature response of respiration across the heterogeneous landscape of the Alaskan Arctic tundra. *J Geophys Res Biogeosci* 123:2287–2302.
34. Huang K, et al. (2014) Impacts of diffuse radiation on light use efficiency across terrestrial ecosystems based on eddy covariance observation in China. *PLoS One* 9:e110988.
35. Thornton PE, Lamarque J-F, Rosenbloom NA, Mahowald NM (2007) Influence of carbon-nitrogen cycle coupling on land model response to CO2 fertilization and cliate variability. *Global Biogeochem Cycles* 21:1–15.
36. Krinner G, et al. (2005) A dynamic global vegetation model for studies of the coupled atmosphere-biosphere system. *Global Biogeochem Cycles* 19:GB1015.
37. Sitch S, et al. (2004) Evaluation of ecosystem dynamics plant geography and terrestrial carbon cycling in the LPJ dynamic global vegetation model. *Glob Change Biol* 9:161–185.
38. Launois T, Peylin P, Belviso S, Poulter B (2015) A new model of the global biogeochemical cycle of carbonyl sulfide–Part 2: Use of carbonyl sulfide to constrain gross primary productivity in current vegetation models. *Atmos Chem Phys* 15:9285–9312.
39. Yang F, Qubaja R, Tatarinov F, Rotenberg E, Yakir D (2018) Assessing canopy performance using carbonyl sulfide measurements. *Glob Change Biol* 24:3486–3498.
40. Bäck J, et al. (2012) Chemodiversity of a Scots pine stand and implications for terpene air concentrations. *Biogeosciences* 9:689–702.
41. Aalto J, et al. (2014) New foliage growth is a significant, unaccounted source for volatiles in boreal evergreen forests. *Biogeosciences* 11:1331–1344.
42. Kooijmans LMJ, et al. (2017) Canopy uptake dominates nighttime carbonyl sulphide fluxes in a boreal forest. *Atmos Chem Phys* 17:11453–11465.
43. Ball JT, Woodrow IE, Berry JA (1987) A model predicting stomatal conductance and its contribution to the control of photosynthesis under different environmental conditions. *Progress in Photosynthesis Research*, ed Biggens J (Springer, Dordrecht, The Netherlands), Vol 4, pp 221–224.
44. Nobel PS (2009) *Physicochemical and Environmental Plant Physiology* (Academic, Oxford).
45. Sun W, et al. (2018) Soil fluxes of carbonyl sulfide (COS), carbon monoxide, and carbon dioxide in a boreal forest in Southern Finland. *Atmos Chem Phys* 18:1363–1378.
46. Mammarella I, Peltola O, Nordbo A, Järvi L, Rannik Ü (2016) Quantifying the uncertainty of eddy covariance fluxes due to the use of different software packages and combinations of processing steps in two contrasting ecosystems. *Atmos Meas Tech* 9:4915–4933.
47. Kolari P, et al. (2009) CO_2 exchange and component CO_2 fluxes of a boreal Scots pine forest. *Boreal Environ Res* 14:761–783.
48. Kooijmans LMJ (2018) Code for "Influences of light and humidity on carbonyl sulfide-based estimates of photosynthesis." Zenodo. Available at https://zenodo.org/record/1211499#.XEC-zFVKgdV. Deposited April 3, 2018.
49. Kooijmans LMJ, et al. (2018) Dataset for "Influences of light and humidity on carbonyl sulfide-based estimates of photosynthesis." Zenodo. Available at https://zenodo.org/record/1211481#.XEC-NVVKhQJ. Deposited April 3, 2018.
50. Sun W (2018) Code for calculation of chamber fluxes: "PyChamberFlux." Zenodo. Available at https://zenodo.org/record/1197330#.XEC-i1VKgdV. Deposited March 13, 2018.